Simple magnetometry with single ion

S. Das,[1] P. Liu,[1] B. Grémaud,[1, 2, 3] and M. Mukherjee[1, 2, 3]

[1] *Centre for Quantum Technologies, National University Singapore, Singapore 117543*
[2] *Department of Physics, National University Singapore, Singapore 117551*
[3] *MajuLab, CNRS-UNS-NUS-NTU International Joint Research Unit, UMI 3654, Singapore*

(Dated: April 5, 2017)

A single trapped and laser cooled ion provides a unique system to perform both precision measurement as well as quantum control over both its internal and external states. The suitability of a trapped ion system as a quantum sensor can hardly be ignored. In this article, we show a simple technique to achieve null magnetic field in a small special volume defined by the confinement volume of a single ion in an ion trap. Unlike, spin precision techniques, this scheme relies on continuously probing dipole transitions, thereby simplifying its implementation. The technique is based on simultaneously occurring three coherent population trapping (CPT) in a null magnetic field. A CPT by its own right is an interesting phenomena and hence it has also been studied theoretically with respect to our 18-level scheme in a singly charged barium ion. The theoretical and experimental comparison of the results clearly shows that the scheme has a potential to improve upon sensing capabilities of small magnetic fields with simple experimental setup.

PACS numbers: 32.70.Cs, 37.10.Ty, 06.30.Ft

arXiv:1704.01070v1 [quant-ph] 4 Apr 2017

INTRODUCTION

Precision measurements and metrology play the central role in our understanding of fundamental physics, material properties, applied physics and technology [1–3, 5]. Atomic clock is an example where technological advancement has pushed the field to develop different technologies which are both competitive as well as complimentary [4]. Similar and even more versatile is the field of magnetic field detection commonly known as magnetometry [5]. Sensing and measuring magnetic field with high precision has numerous applications in the fundamental physics, geo-magnetism, magnetic anomalies in materials, mineral search and in other military applications and medicine [6]. Since magnetic field is a vector field, two types of magnetometers are possible: one which is only sensitive to the magnitude of the magnetic field called the scalar magnetometers and the other which can measure all the vector components separately, known as vector magnetometer. Depending on the hardware used the magnetometers can further be classified as rotating coil and hall effect which are the oldest ones, magneto-resistive device, fluxgate magnetometer, superconducting quantum interference devices (SQUIDS) [7] and Spin-exchange relaxation-free (SERF) atomic magnetometers [8]. The performance of these magnetometers vary depending on the figure-of-merit one is looking at. As an example the SQUID based magnetometers reach sensitivity or the signal-to-noise ratio below 1 $\mathrm{fT}/\sqrt{\mathrm{Hz}}$ [6]. However, the SQUIDs are not simple to deploy due to the stringent requirement of cryogenic environment to operate them usually at 4K or 77K. The only other competing device which can reach such sensitivities are the Spin-exchange relaxation-free (SERF) atomic magnetometers [5]. These devices are based on measuring the spin precession frequency of alkali atoms in low magnetic field and low vapour pressure. In presence of other stray fields the precession frequency is modified and the modification is a measure of the stray field. Despite the achieved high sensitivity, there are essentially two drawbacks: the volume requirement for achieving similar sensitivities as SQUIDs is relatively large and secondly, these devices operate in low magnetic field only thus requiring proper shielding of geo-magnetic field. Therefore, we can see that not all conditions can be fulfilled in one particular device which have complimentary advantages. In particular the sensitivity and resolution are often in contradiction to each other as is obvious from SERF systems which require more volume of gas to enhance the signal-to-noise ratio at the expense of spatial resolution. In very recent advancement a single ion based experiment could provide best of both worlds [9]. However, the cost is the requirement of a clock transition and hence it needs to meet the stringent requirements of an ultra-stable laser. Moreover, stray magnetic field shielding is essential.

Another device which is very similar in hardware as that of an SERF but employs coherent population trapping phenomena to probe the Zeeman splitting in alkali atoms [10, 11]. There are three different modes of operation of this device [13] namely, (i) non-degenerate Zeeman probe where one can measure the Zeeman splitting which is proportional to magnetic field by scanning the frequency of the probe laser (ii) degenerate Zeeman splitting in Hanle type arrangement where one can probe the null magnetic field and use calibrated coils to obtain the vector magnetic field and (iii) polychromatic laser applied to non-degenerate levels similar in spirit but different in application as

(i). The sensitivity of these approaches are comparable to that of SERF but are applicable to a wide range of magnetic field strengths. In particular the degenerate state coherent population trapping method is quite robust as a vector magnetic field probe over a wide range of strengths but it is not an all optical device. There are two methods by which the vector components can be extracted. The first method is by mapping the width and shift of the resonance as a function of magnetic field in transverse and longitudinal directions depending on incoming polarization of the laser. The second method employs calibrated coils to nullify the field components in the three orthogonal directions. However, all these techniques in a cell experiment are limited in sensitivity by the background scattering and also spatial resolution by the required interaction volume. Here we propose an alternative technique to the Hanle type CPT method using single trapped ion. The two basic differences of our proposal as compared to the previous methods are (i) it is a single ion experiment and hence can provide spatial resolution of a few hundred nanometers and (ii) we employ a double lambda type level structure allowing a possible background free measurement. To the best of our knowledge, this is a first application of CPT type scheme with a single ion resolution. In this proof-of-principle approach the achieved sensitivity is only $92\mathrm{nT}/\sqrt{\mathrm{Hz}}$, however we lay down the steps by which it is straight forward to improve on this scheme. We also provide a complete theory of the three CPT resonances that occur simultaneously in our system and match it with our experimental results.

First we discuss the method followed by experimental setup, procedure and results. We conclude by a discussion on some of the straight forward improvements that this new technique may provide and show that the ultimate limit is only shot noise.

METHOD

The basic principle of operation is based on the level crossing spectroscopy [12].

For simplicity we will assume, a five level system with three ground states and two excited state forming a double Λ-type level scheme as shown in figure 1. In our case it is a single$^{138}\mathrm{Ba}^{+}$, however as long as the energy level is similar to any alkaline atom, the scheme can be implemented. The ion is laser cooled via the $\mathrm{S}_{1/2}$-$\mathrm{P}_{1/2}$ transition while fluorescence is observed by continuously exciting the $\mathrm{S}_{1/2}$-$\mathrm{P}_{3/2}$ transition at 455nm simultaneously. In order to avoid in-coherent population trapping into the meta-stable D-levels both the re-pump lasers at 614 nm and 650 nm are simultaneously applied. The rate of emission depends on detuning and intensities of the lasers as well as the strength of the external magnetic field. In the following we will be mainly concentrating on the dependence of fluorescence counts on the magnetic field strength very close to zero. In the special case of zero magnetic field, the Zeeman sub-levels of the D-state are degenerate, this leads to the origin of 4 dark states within the fine-structure Zeeman manifold of the two fine-structure D-states, More precisely, for any value of the laser detuning, for any laser polarization, each of the D-states supports two dark states, which makes the present scheme extremely robust to any experimental imperfections. Therefore one obtains a narrow resonance like feature about the zero magnetic field which is also known as the coherent population trapping [13]. The width of this resonance is mainly governed by the saturation parameters of the re-pumpers provided, the 455nm light is applied with an intensity below saturation. Fundamentally, the width is limited by the combined line width of the applied lasers. While CPT is widely used for magnetometry in gas cell, here it is employed in a single ion. More importantly, due to a single laser cooled ion the CPT features are fundamentally different as compared to CPT in a gas cell. In addition, we observe simultaneously occurring two CPT phenomena in the two fine-structure levels of the D-state which is unique due to the scheme we adopted.

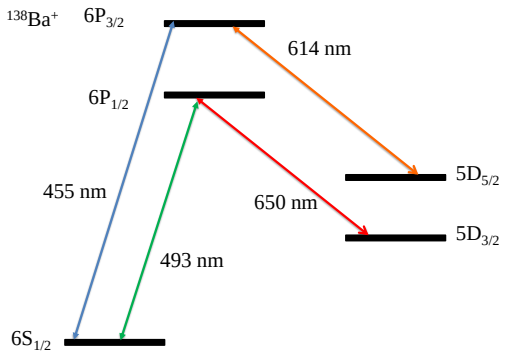

FIG. 1: Lowest relevant energy levels of $^{138}\mathrm{Ba}^{+}$ along with the wavelengths of lasers required to address the relevant transitions. Including the Zeeman sub-levels there are in total 18−levels involved.

From a theoretical point of view, the properties of the fluorescence light are obtained from the stationary solution of the full optical Bloch equations, i.e. including all 18 levels, assuming at diagonal density matrix in the $S_{1/2}$ states for the initial state. In order to extract the ultimate sensitivity of the scheme, the rate of change of the intensity as a function of the applied magnetic field is necessary. The derivative of the fluorescence $\partial I/\partial B$ and its slope $\partial^2 I/\partial B^2$ are obtained from the Taylor expansion of this stationary solution with respect to the magnetic field, i.e. amounting to doing a perturbation

expansion to first and second order. As explained above, the crucial ingredient of the experimental scheme is the existence of a dark state due to a lambda type coupling. A toy model exhibiting the same properties is shown in Fig. 2: the ground state $|g\rangle$ is coupled to the excited state $|e\rangle$ by a first laser (detuning Δ_L), while the two metastable states $|\pm\rangle$ are coupled by the same laser (detuning Δ_P). As long as the two states have the same energy, i.e. $\delta = 0$ corresponding to the dashed lines, they form a perfect two-photon resonant Λ system. In the situation where the two lasers have different detunings ($\Delta_L \neq \Delta_P$), the four level system exhibits one single dark state $(|+\rangle - |-\rangle)/\sqrt{2}$, i.e. fully independent of the different laser parameters. In the stationary regime, the atom is shelved in this dark state and, therefore, is not scattering any photons. As soon as the degeneracy is lifted, there is no dark state resulting in a finite fluorescence. Note that in the case that both lasers have the same detuning, one has the usual tripod configuration with two dark states.

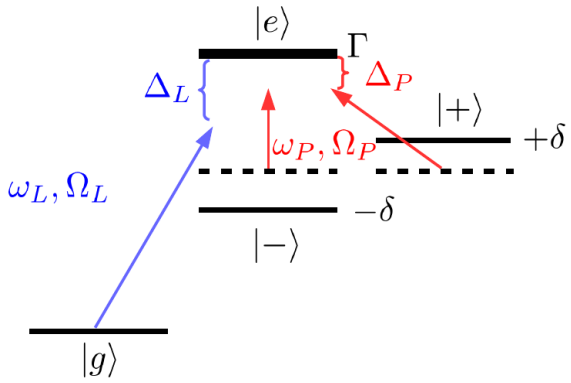

FIG. 2: (Color Online)A schematic diagram of a simple model that exhibits the same feature as the experimental scheme. As long as the two states have the same energy, i.e. $\delta = 0$, they form a perfect two-photon resonant Λ system. In the situation where the two lasers have different detunings ($\Delta_L \neq \Delta_P$), the four level system exhibits one single dark state $(|+\rangle - |-\rangle)/\sqrt{2}$, i.e. fully independent of the different laser parameters. In the stationary regime, the atom is shelved in this dark state and, therefore, is not scattering any photons.

EXPERIMENTAL SETUP

The experiment has been performed on a single ion which provides high spatial resolution for the magnetic field sensing. However, for lower spatial resolution, a cloud of ions or an ion crystal may be used. A schematic of the experimental setup is shown in Figure 3, further detail of the setup can be found in [14, 15]. The main

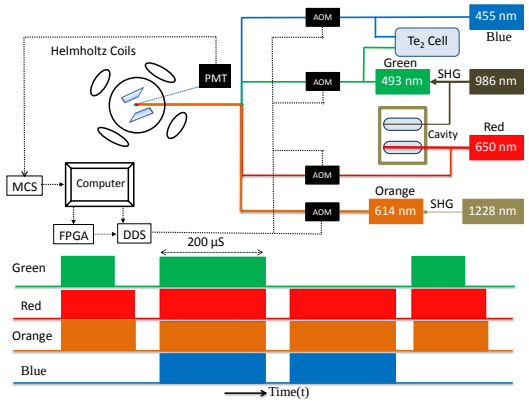

FIG. 3: A Schematic diagram of the experimental setup. The laser frequency and amplitudes are controlled by a acusto-optical modulators. All the laser frequencies are monitored by a wavemeter with 5 MHz resolution. A typical pulse sequence of all the lasers for the measurement is also presented.

components relevant to the present scheme are the ion trap, the excitation lasers and the magnetic field coils. In the following a brief description of these elements are given. The ion trap is a linear Paul trap operating at a secular frequency of about 1 MHz in the radial while few hundred kHz in the axial direction. The ion temperature after Doppler cooling is about 0.5 mK which is sufficient for the present experiment as the Doppler broadening does not play a role. The ion fluorescence signal is detected in a photo multiplier tube after it is filtered by a narrow band interference filter centered at 493 nm or alternatively at 455 nm. The Doppler cooling is usually performed using 493 nm and 650 nm lasers forming a closed cyclic transition. However as we will see in the later section, we have alternatively used 455 nm, 650 nm and 614 nm lasers together to laser cool the ion. The second approach leads to a slightly higher temperature due to the higher width of the $P_{3/2}$ level as compared to the $P_{1/2}$ level. All the lasers are external cavity diode lasers (ECDL) with an estimated linewidth of about 500 kHz. The 493 nm laser is obtained by frequency doubling of a 986 nm ECDL inside a bow-tie cavity. The 614 nm light on the contrary is obtained by frequency doubling a 1228 nm ECDL in a single pass in a wave guide based periodically poled KTP crystal. In this arrangement, the output remains stable due to all fiber based connectivity. In order to minimize the long term drift of the laser frequencies, the 650 nm laser is phase locked to a reference cavity along with 986 nm laser within a same ©zerodure spacer. The 455 nm laser is locked to a tellurium spectral line using modulation transfer spectroscopy (MTS) [16]. The 493nm laser is also be locked to the same tellurium setup as and when needed. The magnetic field at the center of the trapping region is generated by using three

pairs of coils placed in an orthogonal setup as shown in Figure 3 in anti-Helmholtz configuration. This arrangement ensures homogeneity of the field at the trap center within a trapping volume of a few cu.μm. The coils are arranged such that the three mutually perpendicular pairs of coils cancel the earth's magnetic field while another pair of larger coils with a conversion factor of 13.2 G/A are used to produce the magnetic field for the experiment described here.

EXPERIMENTAL PROCEDURE

A single ion is loaded into the trap from a hot barium oven and ionized resonantly using a 413nm ECDL laser at a loading efficiency of about 1 ion/min. Once a successful loading is done, the ion usually remains in the trap for months. The trapped ion is first Doppler cooled and prepared in the ground electronic state. As shown in figure (3), the 455, 614 and 650 nm lasers are simultaneously applied after being combined together in a fiber and injected into the trap for 200 μs. At the same time fluorescence photons emitted at 455 nm are counted via an multi-channel-scalar (MCS) card. As the excitation time is kept large compared to the coherence time in the system, the system attains steady state. For the experiment reported here the polarization of all the lasers are maintained perpendicular to the magnetic field. However, the polarization of the lasers do not play any role in the results which are reported here.

A single aspheric lens placed inside the vacuum chamber collects the fluorescence photons from the ion emitted at 455 nm. In order to suppress the background photons from entering into the detection setup a narrow band interference filter centered at 455 nm is placed before a photo-multiplier tube (PMT). The maximum photon count rate observed is about $70,000$ count/sec on a background scattering rate of about $10,000$ count/sec. The scattering is mainly from the metal electrodes of the trap. As shown in Figure 3, the photon detection setup is placed perpendicular to the excitation laser beams thus observing only spontaneously emitted photons without making any distinction of their polarization. Therefore the configuration is similar to that of an Hanle arrangement but not the measurements.

The saturation parameters of the lasers are experimentally obtained from the fluorescence count measurement as a function of input laser power while all other parameters remaining constant. In case of the 455 nm laser, the saturation parameter is also verified by frequency shift measurement while probing the narrow quadrupole transition between $S_{1/2}$ and $D_{5/2}$ states [17]. The measured saturation intensity obtained from these two methods agree within their respective error of about 4.5 ± 0.5 μW/$100\mu m^2$.

RESULTS

The magnetic field at the position of the ion can be controlled by applying current on individual pair of coils placed in orthogonal arrangement. This allows independent control over the individual vector components of the field. The three vector components are individually calibrated with respect to the coil current along that component. A narrow quadrupole transition between the $S_{1/2}$-$D_{5/2}$ level corresponding to Δm$= 0$ allowed us to measure the linear Zeeman shift as a function of the coil current. Therefore the magnitude of the magnetic field component along that coil direction is derived with a precision of 2.4×10^{-4} G.

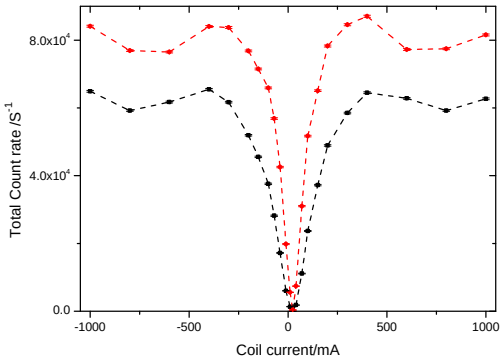

FIG. 4: The fluorescence at 455nm as a function of the vertical component of the magnetic field. The black points are obtained when 493nm laser is also applied on the ion while the red points are obtained when it is off. The dashed lines are used only to guide the eye. The narrow resonance like feature close to the null magnetic field originates due to CPT between the P and D states. The difference in width of the two curves are also reproduced by solving the full Hamiltonian and it points to the saturation of the $P - D$ transitions lasers as is expected in a CPT spectra.

The emitted fluorescence rate at 455 nm as a function of the vertical component of the magnetic field is then plotted as shown in Figure 4. The dashed curve is obtained when 493 nm laser is also applied on the ion while the solid line is when it is off. The full curve for higher magnetic field is rather very complex as it involves optical nutation due to the coherence of the lasers interacting with 18-levels of the ion. We have performed however numeric calculation of this Hamiltonian which turned to be a difficult fit to the experimental data keeping minimal free parameters. Indeed, from the numerical computations, it turns out that the width of the dip is generally

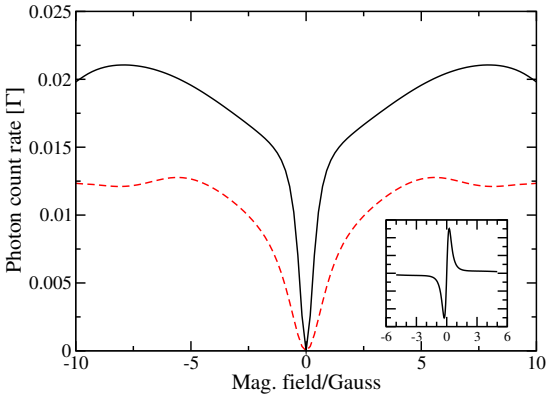

FIG. 5: (Color online)Numerical results for the fluorescence at 455nm as a function of the vertical component of the magnetic field. The dashed curve is obtained when 493 nm laser is also applied on the ion while the solid line is when it is off. The inset displays the derivative of the fluorescence when the 493 laser is off. The agreement with the experimental results when the 493 laser is on or off is rather good. On the other hand, the behavior of the curves away from the CPT resonance, is not entirely captured by the numeric calculation due to fewer available experimental points.

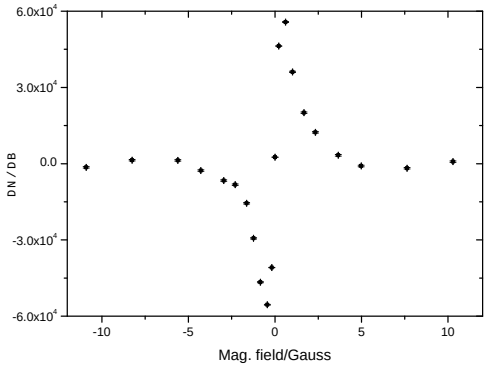

FIG. 6: Derivative of the fluorescence at 455nm as a function of the vertical component of the magnetic field when 493 nm laser is off.

independent of the laser detunings and only weakly dependent of the saturation parameters of the 614 nm and 650 nm lasers, whereas the wings, i.e. the behavior further from the CPT resonance, depend strongly on all the lasers parameters namely coherence, detuning and saturation. Nevertheless, we have found a qualitative agreement with the experimental results as shown in Fig. 5. The numerical values for the different laser are: saturation of the 455 nm (614 nm, 650 nm and 493 nm) is 0.5 (15, 40 and 5 (when on) respectively) and the detuning of the 455 nm (614 nm, 650 nm and 493 nm) is -10 MHz (-50 MHz, -40 MHz, -20 MHz). The most important feature for our present discussion is the central dip close to the zero magnitude of the magnetic field.

At exact null magnetic field, the atom is transparent to all the laser lights and no fluorescence is observed except only background scattering level. As explained by the simple model, the atom ends up in one of the dark states as soon as the magnetic field is null which makes the magnetic sub-levels degenerate. Since the D-states are only coupled by quadrupole transitions, the width of this dip or the slope of $\partial I/\partial B$ at $B = 0$, is mainly governed by the saturation parameter of the re-pump lasers.

Here we discuss the three major differences in the spectral feature in our experiment as compared to a gas cell experiment [13]. First, unlike a gas cell experiment with the Hanle type CPT induced by zero magnetic field, our experiment with a single atom does not show any shift due to the longitudinal or transverse magnetic field. It is completely symmetric and hence only three axis coil current scan to nullify the magnetic field in three orthogonal direction allows the measurement of the vector field. In a gas cell the shift of the resonance center in presence of a longitudinal magnetic field along the light propagation direction originates due to the velocity distribution of the free atoms. In a single ion experiment confined in a trap cooled to Doppler limit, there is no net shift in the spectrum. Second, in our experiment, there are three possible CPTs depending on the relative laser detunings. Therefore in one configuration it is possible to achieve shot noise limited sensitivity. In case of a gas cell experiment with the best possible scheme, the sensitivity is limited by the background light scattering which is usually removed by a lock-in type measurement. Last but not the least, the measurement volume of a single ion is determined by the single ion confinement volume, which under Doppler limit is a few hundred micrometers cube. This is orders of magnitude lower as compared to small gas cells and hence can provide high spatial resolution.

Now we provide some of the key figures-of-merit for our present system used as a proof-of-principle experiment. As shown in Figure 6, the derivative of the narrow dip provides a zero crossing with a slope $(\Delta N/\Delta B)$ of 1.17×10^5 counts/s/Gauss. The present background noise $(\sigma(N))$ is 1.07×10^2 counts/s. Thus the sensitivity which is define as

$$\Delta B = \sigma(N)/(\Delta N/\Delta B), \qquad (1)$$

is about 92 nT/$\sqrt{\text{Hz}}$. Since these measurements are taken as a proof-of-principle, the accumulation time is not optimized. The range of magnetic fields that can be probed depends on the required coil current to compensate the external field. In our measurement, the external field is the geomagnetic field in addition

to laboratory stray fields. The measured value of the vertical component of the local magnetic field at the position of the ion is found to be 310 ± 10 mG. The uncertainty is dominated by the saturation of the re-pump laser in this measurement. These are experimental uncertainties but not the accuracy of the system. In the following we provide some of the improvements that can be implemented in order to compete with the present state-of-the-art vector DC magnetometers working over a wide range with nanometer order spatial resolution.

The first improvement is to observe the background free-spectra from the $P_{1/2}$-$S_{1/2}$ transition which is at 493 nm. This would involve the same scheme but instead of observing the 455 nm photons, the observation will be performed on the 493 nm spontaneously emitted photons in absence of any 493 nm laser excitation. Thus, the sensitivity can be improved without much cost to the signal. At present the width of the CPT is dominated by the re-pump laser intensity. Therefore the other improvement which can be easily implemented is to reduced the intensity of the re-pump lasers. On one hand it will reduce the rate of emission, but on the other hand it will improve the sensitivity by increasing the slope of the dispersion curve. This is shown in Fig 7 which is obtained by computing the second order coefficient in the Taylor expansion of the fluorescence as a function of the magnetic field. From a theoretical point of view, this amounts to doing a perturbation expansion up to the second order of the stationaty solution of the optical Bloch equation. A detailed analysis of the behavior of the slope of the dispersion curve is beyond the scope of this paper and will be presented elsewhere.

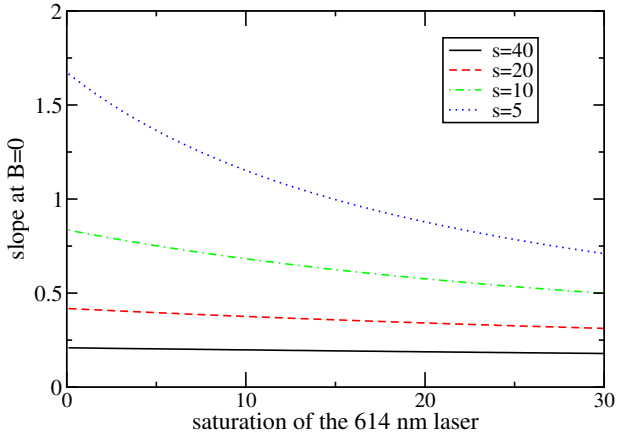

FIG. 7: (Color online) Numerical value of the slope of the derivative of the fluorescence at 455nm as a function of the saturation parameter of the 614 nm laser and for different values of the saturation of the 650 nm laser. As one can see, lowering the repumper intensities is increasing the slope of the dispersion curve and, thereby, the sensitivity of the experiment.

The magnetometer described here, can also be used to precisely generate a physical volume with null magnetic field with active locking to the zero crossing of the dispersion signal. This is essential in many experiments related to the ion trap quantum computers, zero-field nuclear magnetic resonance magnetometers and other magnetometers which require expensive passive shielding to get rid of the environmental noise.

CONCLUSION AND OUTLOOK

We conclude that our proposed new scheme of a double CPT type magnetometer with a single ion can provide both high spatial resolution as well as high sensitivity, yet without the need of any narrow band clock laser. The proof-of-principle experiment has sensitivity of only 92 $\mathrm{nT}/\sqrt{\mathrm{Hz}}$ without any optimization but has the potential to be competitive to other state-of-the-art magnetometers. It has a wide range of operation and no stringent requirement on the lasers, thus the scheme is adoptable to other existing hardware.

[1] C. S. Wood *et al.*, Science **275**, 1759 (1997).
[2] K. Tsigutkin, D. Dounas-Frazer, A. Family, J. E. Stalnaker, V. V. Yashchuk, D. Budker, Phys. Rev. Lett. 103, 071601 (2009).
[3] M. Mukherjee *et al.*, Phys. Rev. Lett. **93**, 150801 (2004).
[4] A. D. Ludlow, M. M. Boyd, J. Ye, E. Peik, and P.O. Schmidt Rev. Mod. Phys. 87, 637 (2015).
[5] D. Budker and M. Romalis, Nature Physics 3, 227 (2007).
[6] I. K. Kominis, T. W. Kornack, J. C. Allred and M. V. Romalis, Nature 422, 596 (2003).
[7] R. C. Jaklevic, J. Lambe, A. H. Silver and J. E. Mercereau, Phys. Rev. Lett. 12 159 (1964).
[8] J. C. Allred, R. N. Lyman, T. W. Kornack, M. V. Romalis, Phys Rev Lett. 89, 130801 (2002).
[9] I. Baumgart, J.-M. Cai, A. Retzker, M. B. Plenio, and Ch. Wunderlich, Phys. Rev. Lett. 116, 240801 (2016).
[10] J. Belfi, G. Bevilacqua, V. Biancalana, S. Cartaleva, Y. Dancheva, and L. Moi, J. Opt. Soc. Am. 24, 2357 (2007).
[11] V. I. Yudin, A. V. Taichenachev, Y. O. Dudin, V. L. Velichansky, A. S. Zibrov, and S. A. Zibrov, Phys. Rev. A 82, 033807 (2010).
[12] P. A. Franken, Phys. Rev. 121, 508 (1961).
[13] E. Alipieva *et al.*, Proc. of SPIE 5830, 170 (2005).
[14] D. De Munshi, T. Dutta, R. Rebhi, and M. Mukherjee, Phys. Rev. A **91**, 040501(R) (2015).
[15] Tarun Dutta *et al.*, Sci. Rep. 6, 29772 (2016).
[16] T. Dutta, D. De. Munshi, M. Mukherjee, J.Opt.Soc.Am. **B33**, 1177-1181 (2016).
[17] D. Yum, D. De Munshi, T. Dutta, M. Mukherjee, arXiv:1611.10016 (2016).